

Kamiokande and Super-Kamiokande

Yoichiro Suzuki

*Kamioka Observatory, Institut for Cosmic Ray Research, The University of Tokyo, Higashi-Mozumi,
Kamioka-chou, Gifu, 560 Japan*

Neutrino astrophysics has begun in 1987 when Kamiokande observed the neutrino burst from a supernova SN1987A. Kamiokande succeeded to observe solar neutrinos and demonstrated at the first time that the observed neutrinos are coming from the direction of the sun and confirmed the long standing solar neutrino problem. The atmospheric neutrino anomaly was first pointed out by the Kamiokande experiment in 1988 and is now thought to be an evidence of a neutrino oscillation. Super-Kamiokande, the bigger successor of Kamiokande, started its operation in April 1996. The accumulated data have already exceeded those of Kamiokande in its quality and quantity. New insights into neutrino masses will be obtained from the results of SK in very near future.

1 Introduction and Detector

The gigantic imaging water Cherenkov detectors located 1000 m underground (2,700m water equivalent), Kamiokande [1] and Super-Kamiokande [2], are the powerful tool to understand neutrino properties and study proton decay. The volume of Kamiokande (KM) is 4,500 tons (948 photomultiplier tubes (PMTs) are arranged to watch inner volume of 2,140 tons), and that of Super-Kamiokande (SK) is 50,000 tons (11,146 PMTs are arranged for the inner volume of 32,000 tons). KM has started its operation in 1984, primarily to study nucleon decay [3] and later in 1987, KM has upgraded to be able to detect low energy events above 9.3 MeV to study solar neutrinos. In February, 1987, just after the upgrade, KM has observed the neutrino bursts from a supernova SN1987A [4] exploded in the Large Magellanic Cloud, 160 kilight years away. This is the first observation of astrophysical neutrinos other than solar neutrinos, and is the beginning of neutrino-astronomy. KM has succeeded to obtain a finite solar neutrino flux in 1987, soon after the neutrino burst detection. This observation provided the first evidence that the sun creates high energy neutrinos produced by the 8B decay and confirmed the solar neutrino problem [5]. Unexpected anomaly of the atmospheric neutrinos, which is now thought to be an indication of a neutrino oscillation was first pointed out by the KM experiment in 1988 [6]. KM has stopped major physics run in February in 1995 and stopped its operation in summer 1997. The last stage of the experiment is solely devoted to a supernova watch. The physics achievements and the history of KM are summarized in references [7][8].

Since the space is limited in this paper, we mostly discuss about the SK experiment in the following parts and physics discussions will also be limited to neutrino oscillation studies.

The schematic view of the SK detector is shown in figure 1. SK is not only bigger than KM in its size but also has better energy, position and directional resolutions 14% (19%), 26° (27°), 87cm (100cm) for 10 MeV electrons respectively (the numbers shown in the parentheses are those for KM). The better resolutions are achieved by the increased number density of PMTs. The PMTs are arranged on the inner surface of the detector with the density of 2 PMTs / 1 m² (1 PMT / 1 m² for KM) which covers the 40% of the inner surface. This arrangement more than compensates the light loss (due to the attenuation) of the longer travel distance of the Cherenkov light than KM. Outside of the

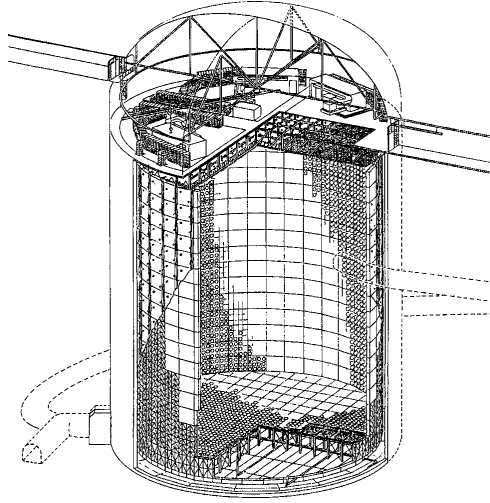


Figure 1: A schematic view of the 50,000 ton imaging water Cherenkov detector, Super-Kamiokande. The detector is a cylindrical shape, 39.3m in diameter and 42m in height. The inner volume of 32,000 tons, 16.9m in radius and 36.2m in height, is viewed by 11,146 photomultiplier tubes with 50 cm diameter.

The inner detector is surrounded by the outer detector of 2m thick active water slab viewed by 1,185 20 cm PMTs. This provides the shield against the external gamma rays and neutrons, and positively identifies incoming particles like throughgoing cosmic ray muons, particles exiting the detector and so on.

The energy of neutrinos, which we are interested in detecting in SK, ranges from a few MeV to more than 100 TeV. The interactions of neutrinos in the detector will be described later for solar and atmospheric neutrino cases.

The relativistic charged particles traversing faster than the light velocity in the water emit Cherenkov lights with an angle of

$$\cos\theta = \frac{1}{\beta n},$$

where $\theta=42^\circ$ for particles with $\beta=1$, and n is the refractive index of water. These ring image Cherenkov lights are detected by the PMTs. The hit pattern, pulse height and timing information are used to reconstruct event vertex, direction, energy and particle species. The details of the event reconstruction can be found in one of these theses[9].

2 Operation and Calibration

Super-Kamiokande (SK) has started the operation on 1st of April in 1996 and been continuously taking data with the cumulative live-time close to 90%. Most of the time not for taking data are spent to calibrations, especially to those using electron LINAC [10].

Water is essential for the SK experiment. It serves as a target. But the light scattering and absorption affects on the energy resolution, vertex resolution and so on. For the first two months after the start-up there was a rapid improvement of the water transparency, since we had just started to circulate the water a few days before the start-up. Therefore in the analysis presented here we have not used the data taken in April and May, 1996. There is a small change of the water transparency during the experiment. The water transparency, which is about 100m at 40m now is monitored and measured by several methods: muon decay γ electrons, throughgoing muons and a direct measurement.

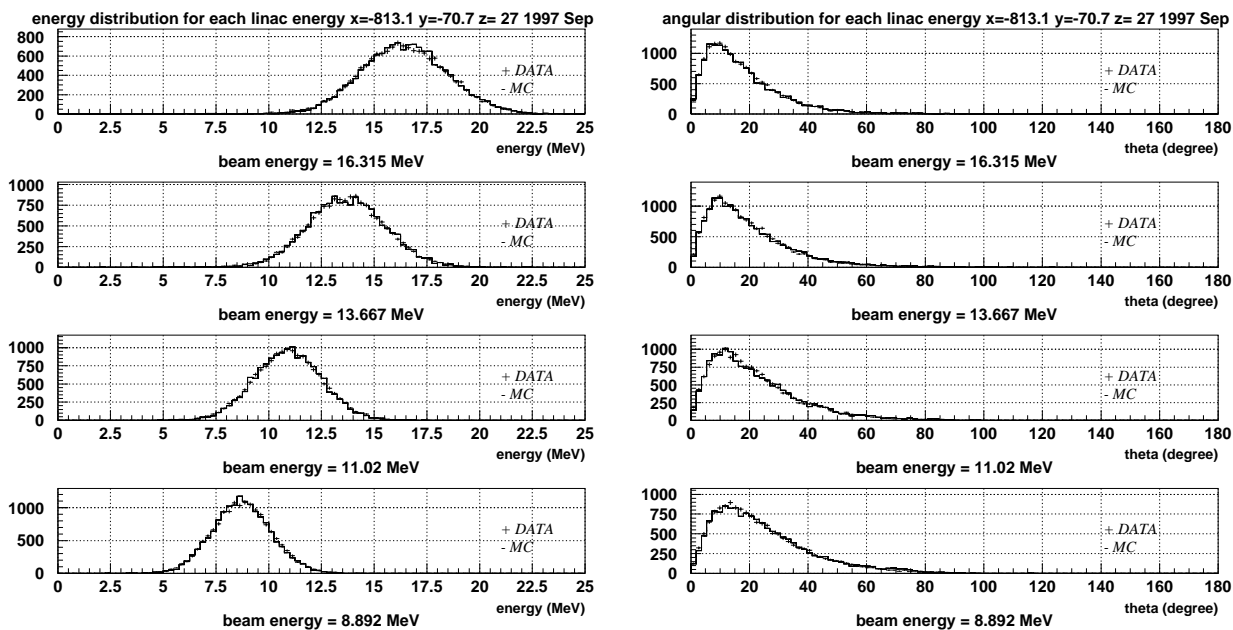


Figure 2: The energy distribution of LINAC data taken at the central height of the detector, but with about 8m off the center towards the side wall. The energies of the electrons are at 16.3, 13.7, 11.0 and 8.9 MeV from the top figure to the bottom figure. The results from the MC simulations are also shown by the solid lines. The data and the MC agree very well.

Figure 3: Same as figure 2, but for the angular distributions.

using a Dye laser and a CCD camera. A change of the water transparency was taken into account when the event energy was reconstructed.

Another important element related to the water quality is Radon concentration in the water. The daughter of the Radon decay (^{214}Bi) emits β rays with the maximum energy of 3.26 MeV and the resolution of the detector is the major background for the solar neutrino measurement. The current concentration of Rn in the water is measured to be less than a few Bq/m³ which is already more than an order of magnitude higher than the KM level but is still below the background. We are making extensive efforts to make further reduction of Rn in the water. Analysis threshold of 5 MeV current is mainly determined by this background level.

Triggers are made by the number of PMT hits with the 200 ns event window. Data are being taken with two threshold levels — the low energy (yLE) and the super-low energy (ySLE) triggers. The threshold of the LE triggers is ~ 29 hits or corresponding to about 5.7 MeV on an average. The SLE triggers are set at 24 hits (4.0 MeV on an average). The event vertex of those events only having SLE triggers are quickly reconstructed in a crude fiducial target applied to the on-line host computer. This selection reduces the 10 Hz SLE trigger to about 5 Hz which is a small portion of the 1 Hz of the LE trigger.

The energy of an event is determined either by the high energy (atmospheric neutrino) and low energy (solar neutrino) events. In the atmospheric neutrino analysis, the energy is determined based on the number of photo-electrons (response approximately corresponds to 1 MeV) and the solar

neutrino analysis the energy is determined by the number of hit PMTs since in such low energy most of the PMT hits are one photoelectron (5.6 hits approximately corresponds to 1 MeV).

The accuracy of the energy scale for high energy events is estimated to be $\pm 2.4\%$ by the various methods by using cosmic ray through-going muons, stopping muons, muon-decay electrons, various mass of π^0 s and so on. The energy resolution for electrons and muons are $2.5\%/\sqrt{E(\text{GeV})} + 0.5\%$ and 3% respectively.

In the solar neutrino analysis the absolute energy of the events is calibrated by using the electron beam produced by the electron LINAC placed at the SK tank, which covers the energy range between 5 and 15 MeV, exactly matching to the energy spectrum of the solar neutrinos. The LINAC was also used to obtain the angular resolution and the vertex resolution. The beam energy of the LINAC was calibrated by the germanium detector which was calibrated by using the mono-chromatic electrons selected by a magnetic spectrometer. The typical energy and angular distribution taken at various energies and at the injection position of about 8 m from the wall are shown in figures 2 and 3.

The uniformity throughout the entire fiducial volume and the directional dependence were checked by the LINAC data taken at different positions, ray sources using $\text{Ni}(n,\gamma)\text{Ni}'$ reactions placed in many different places in the detector and the palladium events which happen uniformly in the detector volume. After considering those effects the energy scale error of the total flux measurement is estimated to be $\pm 0.85\%$. The detail of the calibration will be found in ref [10][18].

3 Physics with Super-Kamiokande

The primary physics subject of Kamiokande (KM) is a search for nucleon decay; the name Kamiokande comes from Kamioka Nucleon Decay Experiment. After the observation of the neutrino burst from SN1987A and the success of the solar neutrino measurement, people would call the experiment as Kamioka Neutrino Detection Experiment.

The main purposes of Super-Kamiokande (SK) are, of course, to search for nucleon decay with an order of magnitude better sensitivity to measure neutrinos from the sun and to study atmospheric neutrinos.

If neutrinos have finite masses and non-zero mixings among mass eigen-states, then neutrinos produced at the flavor eigen-states may oscillate among different states with the following probability (for two neutrino oscillation case),

$$P(\nu_\alpha \rightarrow \nu_\beta) = \sin^2 2\theta \sin^2 \left(1.27 \cdot \Delta m^2 \cdot L/E \right),$$

where E is the energy of neutrino and L is the distance between the source and the detector and E and L are determined by the experimental arrangement. If $\Delta m^2 \gg E/L$, then $P(\nu_\alpha \rightarrow \nu_\beta) = \frac{1}{2} \sin^2 2\theta$, and if $\Delta m^2 \ll E/L$, then experiments hardly see the oscillation effect and are able to set the upper limit by $\sin^2 2\theta \cdot \Delta m^2 \ll 0.8 [E/L] \sqrt{P(\nu_\alpha \rightarrow \nu_\beta)}$. If $\Delta m^2 \sim E/L$, experiments are in a most optimum position. For example, for a configuration $E \sim 1 \text{ GeV}$ and $L \sim 10$ to $10,000 \text{ km}$ (in the case of the sub-GeV atmospheric neutrinos) $\Delta m^2 \sim 10^{-1} \sim 10^{-4} eV^2$ and for $E \sim 10 \text{ MeV}$ and $L \sim 150,000,000 \text{ m}$ (for 'Just So' solar neutrino oscillation) $\Delta m^2 \sim 10^{-11} \sim 10^{-10} eV^2$.

When neutrinos pass through the media, the electron neutrino obtains an additional potential, $\sqrt{2} G_F n_e$ through the charged current forward scattering amplitude. The equation of the neutrino

propagation for $\nu_e \rightarrow \nu_\mu$ case is,

$$i \frac{d}{dt} \begin{pmatrix} \nu_e \\ \nu_\mu \end{pmatrix} = \begin{pmatrix} -\frac{\Delta m^2 \cos 2\theta}{4p} + \sqrt{2} G_F n_e & \frac{\Delta m^2 \sin 2\theta}{4p} \\ \frac{\Delta m^2 \sin 2\theta}{4p} & \frac{\Delta m^2 \sin 2\theta}{4p} \end{pmatrix} \begin{pmatrix} \nu_e \\ \nu_\mu \end{pmatrix}.$$

The mixing angle in the matter becomes,

$$\tan 2\theta_m = \frac{\tan 2\theta_V}{1 - (2p\sqrt{2}G_F n_e)/\Delta m^2 \cos 2\theta_V}.$$

If $(2p\sqrt{2}G_F n_e)/(\Delta m^2 \cos 2\theta_V) = 1$ (resonance condition) then the mixing angle in the matter becomes maximal, even though the vacuum mixing angle is small. If the neutrino propagates adiabatically through the resonance region, electron neutrino converts into ν_μ 's. For 10 MeV neutrino produced in the sun, it is the resonance condition when pass through the sun ($0 < n_e/N_A < 100$) if

$$\Delta m^2 \leq 1.6 \times 10^{-4} eV^2.$$

Adiabatic condition for the 10 MeV neutrinos,

$$\Delta m^2 \frac{\sin^2 2\theta}{\cos 2\theta} \geq 6.3 \times 10^{-8} eV^2.$$

These conditions determine the parameter region explaining the 'observed' conversion rate.

Searches for neutrino masses have been done not only by the neutrino oscillation experiments, but also by other methods like direct mass searches and double beta decay experiments although the indication of the finite neutrino masses only come from oscillation experiments. The current upper limit on the neutrino mass from the experiments looking directly for the evidence of finite neutrino masses are,

$$m_{\nu_\tau} \leq 18.2 MeV/c^2 [12]$$

$$m_{\nu_\mu} \leq 170 keV/c^2 [13]$$

$$m_{\nu_e} \leq 3.5 \sim 5.6 MeV/c^2 [14]$$

The best limit for the Majorana neutrino masses of $0.48 \sim 1.5 eV^2$ [15] was obtained from the double beta decay experiment (We have included the uncertainty of the nuclear matrix element).

As you see above, neutrino oscillation is the only way to approach small masses (difference) well below 1 eV: sensitive to the very wide Δm^2 range down to $10^{-12} eV^2$.

The neutrino oscillation studies in SK will be done not only with high statistics and better quality but with different approaches: model independent and flux calculation independent analyses are the key issues for the SK experiment.

3.1 Atmospheric Neutrinos

Atmospheric neutrinos are produced in the upper atmosphere through the decay of mesons produced by interactions of primary cosmic rays on nuclei in the atmosphere. The neutrino energy ranges from below GeV to over TeV and the distance from the points where neutrinos are produced and the detector location ranges from 10 to 13,000 km. Therefore the sensitivity to the mass differences down to $\Delta m^2 \sim 10^{-4} eV^2$.

At the low energy limit where most of the muons produced in the atmosphere decay, the ratio of $(\nu_\mu + \bar{\nu}_\mu)/(\nu_e + \bar{\nu}_e)$ becomes ~ 2 . The more the energy increases, the more the ratio becomes larger.

The uncertainty of the atmospheric neutrino flux calculations is mainly come from the uncertainty of the primary cosmic ray flux, meson productions, and neutrino interactions, and is estimated to be $\sim 25\%$ (20% from the flux and 15% from the interaction uncertainties). In order to minimize those uncertainties in the neutrino oscillation studies, the double ratio $R = (\mu/e)_{data} / (\mu/e)_{MC}$ is usually taken.

Another important approach is to study the zenith angle distribution of the neutrino events which will be described later.

In SK the atmospheric neutrinos are studied by two classes of the events: the contained events and upward going muons. The upward going muons are produced by high energy muon neutrino interactions taken underneath of the detector and penetrating the detector entering from the bottom of the detector. We will not discuss the upward going muons in this paper.

3.1.1 Contained events

The contained events are those produced in the detector by neutrino interactions. Traditionally we divide the contained events into sub-GeV ($E_l < 1.33$ GeV) and multi-GeV ($E_l > 1.33$ GeV). The sub-GeV samples were used originally to search for proton decay.

The strategy to study atmospheric neutrinos is to identify neutrino flavor through the identification of the lepton flavor of single ring events (in the sub-GeV sample) and of most energetic particle (in the multi-GeV sample). In the multi-GeV sample we have also included so called partially contained events (PC)—events which have one track exiting from the inner detector. For example, 91.1% of the electron events come from ν_e charged current interactions and 95.9% of the muon events come from ν_μ charged current interactions in sub-GeV sample. For the multi-GeV sample, the correlation is much better. Therefore the particle identification is the key issue for the neutrino oscillation analysis.

The data between May-27 in 1996 and Oct-16 in 1997 (414.2 effective live days) are used for the present analysis. The contained events are first selected by applying simple computer algorithm to the raw data ($\sim 10^6$ events/day): (1) no significant outer detector activity, (2) the inner total charge is > 200 photo-electrons. We have also applied further cuts to remove stopping muons, through going muons and electrons from stopping muon decays. This reduction step yields ~ 30 events/day for the fully contained event (FC) selection and ~ 20 events for partially contained event (PC) selection. Then the events were scanned by two independent physicists and the remaining background events were rejected. We finally obtained ~ 8.0 fully contained events/day and ~ 0.5 partially contained events/day after applying the 2m cut from the inner PMT surface (22.5kt on fiducial volume) and the minimum energy cuts of 30 MeV (fully contained) and 3,000 photo-electrons (partially contained).

The identification of electron and muons are done by using the information of the diffuseness of the Cherenkov rings. The probability is defined by

$$P_{e(\mu)}^{(1)} = \prod_{\theta_i < 1.5\theta_c} \frac{1}{\sqrt{2\pi}\sigma_i} \exp \left[-\frac{1}{2} \left(\frac{p \cdot e^i - p \cdot e_{e(\mu)}^i}{\sigma_i} \right)^2 \right],$$

where σ_i is the resolution of PMT including also an effect of the gain spread. We have also similar probability function for the angular distribution, $P_{e(\mu)}^{(2)}$. Then the log-likelihood function is determined by

$$\mathcal{L} = \log(P_\mu^1 \cdot P_\mu^2) - \log(P_e^1 \cdot P_e^2).$$

The likelihood distribution of the particle identification is shown in figure 4 and you can clearly see the good separation between the μ -like and e -like events. The mis-identification probability is estimated

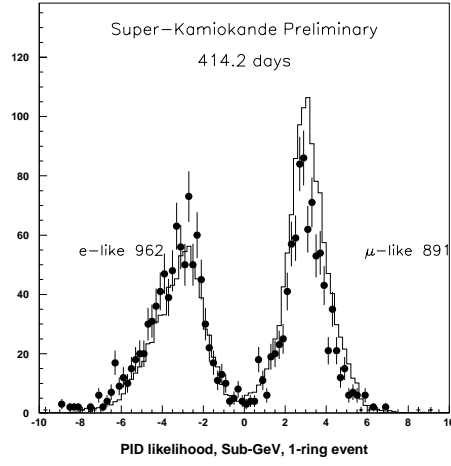


Figure 4: The distribution of the likelihood to identify electrons and muons. The separation between μ -like and e -like events are clearly seen. The probability of the misidentification is less than 1%.

Table 1: The summary of the contained events caused by the atmospheric neutrino interactions in Super-Kamiokande for 414.2 effective days. Also listed is the predictions by the Monte Carlo Calculation.

	Sub-GeV		Multi-GeV	
	DATA	MC(Honda)	DATA	MC(Honda)
1R	1853	2001.3	394	411.6
e-like	962	796.1	218	182.7
μ -like	891	1205.2	176	229.0
2R	594	657.2	153	143.7
$\geq 3R$	155	190.1	151	156.3
PC			200	244.8

to be less than 1%. The validity of the particle identification was verified by the test done at KEK using a 1kt water Cherenkov detector by the electron and muon beam with known momentum [16].

The results after the final data selections are summarized in table 1. All the events are used to make the double ratio of the muons and electrons:

$$\frac{(\mu/e)_{DATA}}{(\mu/e)_{MC}} = 0.635^{+0.029}_{-0.028} \pm 0.009 \pm 0.048 (sub-GeV),$$

$$\frac{(\mu/e)_{DATA}}{(\mu/e)_{MC}} = 0.665^{+0.059}_{-0.054} \pm 0.020 \pm 0.078 (multi-GeV (FC)),$$

$$\frac{(\mu/e)_{DATA}}{(\mu/e)_{MC}} = 0.664^{+0.069}_{-0.062} \pm 0.022 \pm 0.097 (multi-GeV (FC + PC)).$$

The first, second and third errors come from statistics, MC statistics and systematics, respectively. The double ratios, $(\mu/e)_{DATA}/(\mu/e)_{MC}$, as a function of the energy for sub-GeV and multi-GeV sample are shown in figures 5 and 6. The nonmonotonous suppression of $\sim 60\%$ is seen over entire energy region.

The zenith angle distribution, which is of most importance to understand about neutrino oscillations, is similar to the E/L plot since the zenith angle, θ_z , approximately determines the distance (L)

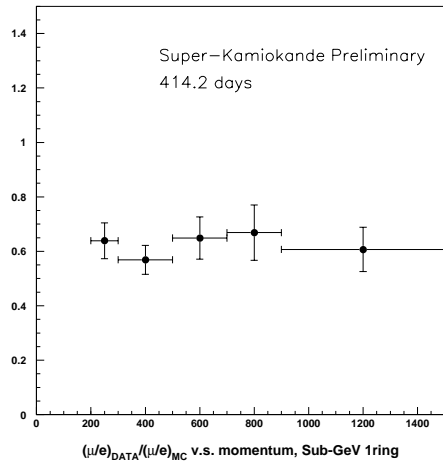


Figure 5: The double ratios, $(\mu/e)_{DATA}/(\mu/e)_{MC}$, for the sub-GeV sample as a function of energy for 414.2 days of data.

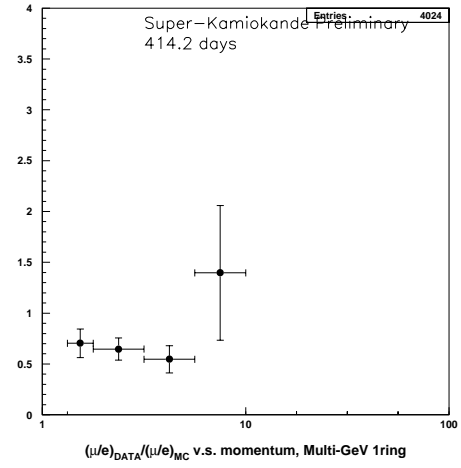


Figure 6: Same as figure 5, but for the multi-GeV data sample.

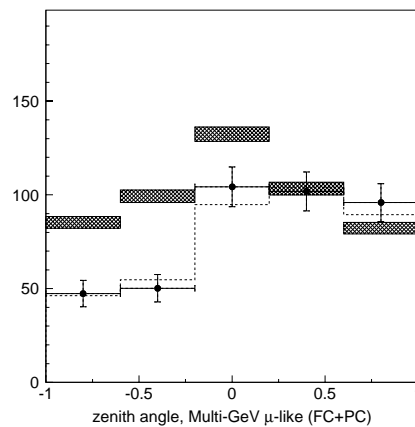
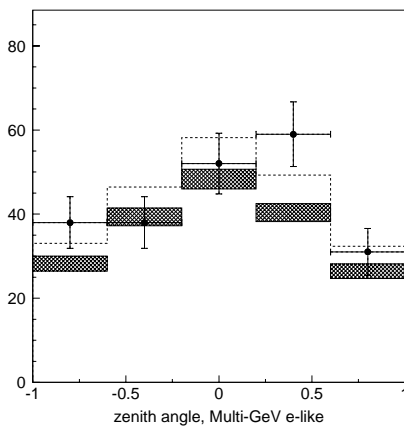
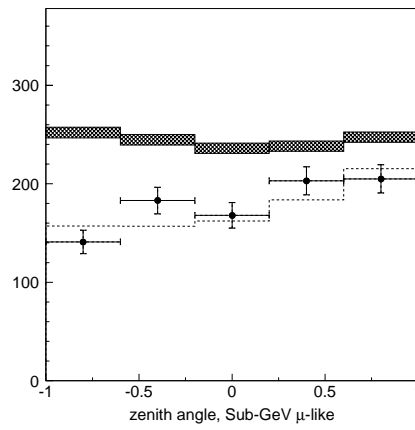
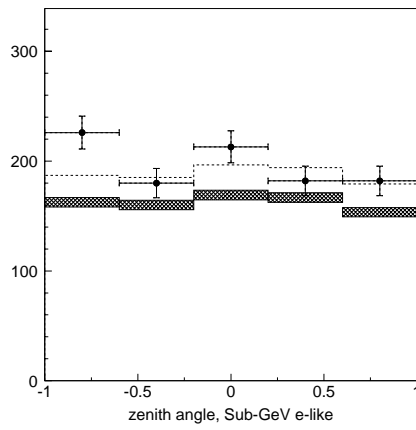


Figure 7: The zenith angle distribution of the e-like and μ -like events for the sub-GeV and multi-GeV data samples. The solid bars show the prediction from the MC calculation (no oscillation) being symmetric for all the distributions. In the high energy muon sample, the zenith angle distortion is prominent. The predicted distributions for the neutrino oscillation $\nu_\mu \rightarrow \nu_\tau$ ($\Delta m^2 = 5 \times 10^{-3} eV^2$, $\sin^2 2\theta = 1.0$) are also shown by the dotted lines. For e-like data, the difference between no oscillation (solid bars) and the oscillation (dotted) comes from the flux re-normalization due to the absolute flux uncertainty of 25%.

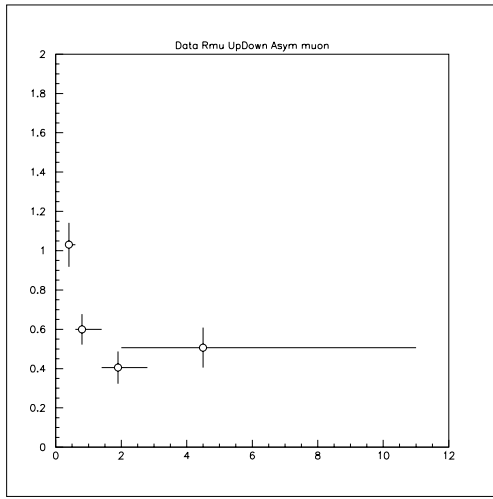


Figure 8: The up/down ratio of the upward going ($-1 < \cos\theta_z < -0.2$) and downward going ($0.2 < \cos\theta_z < 1.0$) events for the μ -like events. The horizontal axis shows the 'neutrino' energy estimated with the help of the MC calculations. The lowest data less than 500 MeV should always be symmetric (in this figure) since here is poor angular correlation between leptons and neutrinos in this energy region.

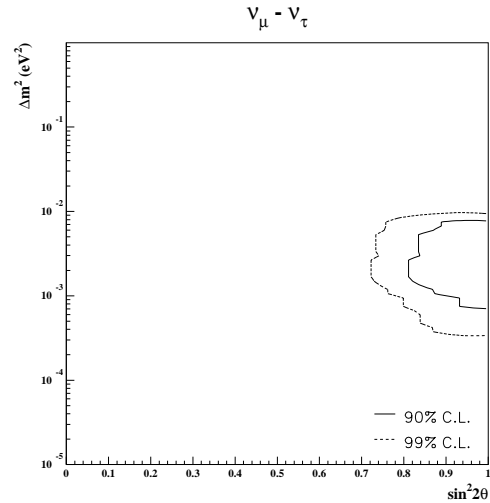


Figure 9: An Allowed region assuming $\nu_\mu \rightarrow \nu_\tau$ neutrino oscillation.

between the detector and the place where neutrinos are produced. If you see the distribution, a non-immediate electric dipole moment value of the oscillation parameter. Another important characteristic is that the zenith angle distribution should be symmetric.

This nature of the symmetry does not depend upon any flux calculation or size of a small difference (less than 3% for the events below 1 GeV; negligible above 1 GeV) of the geo-magnetic cut-off. Therefore, any up/down asymmetry found, indicates immediately that some unknown situations exist in this sense that stand by itself.

In figure 7, we have shown the number of e -like and μ -like events as a function of zenith angle for the sub-GeV and multi-GeV datasets. The prediction shown by the solar flare is symmetric for all but the data at small angles, though the predictions have 25% systematic error which are not shown in figure 7. The electric sample shows more or less symmetric distribution in the muon sample. It is evident that more neutrinos come from the top of the detector and less from the bottom of the detector. The multi-GeV data has most prominent characteristics.

In order to magnify the problem, we have shown in figure 8, the ratio of the upward going ($-1 < \cos\theta_z < -0.2$) and downward going ($0.2 < \cos\theta_z < 1.0$) events for the μ -like events. All the data except the less than 500 MeV are $\sim 50\%$. The lowest data less than 500 MeV should always be symmetric since here is poor angular correlation between leptons and neutrinos in this energy region. Therefore, the data below 500 MeV can be used as a control sample and should be 1 in figure 8.

By using the information on the energy and zenith angle distribution, we can get a confidence contour of the neutrino oscillation parameter (for $\nu_\mu \rightarrow \nu_\tau$ case) shown in figure 9. The expected zenith angle distribution for $\Delta m^2 = 5 \times 10^{-3} eV^2$, $\sin^2 2\theta = 1$ are shown in figure 9. The figure shows that the

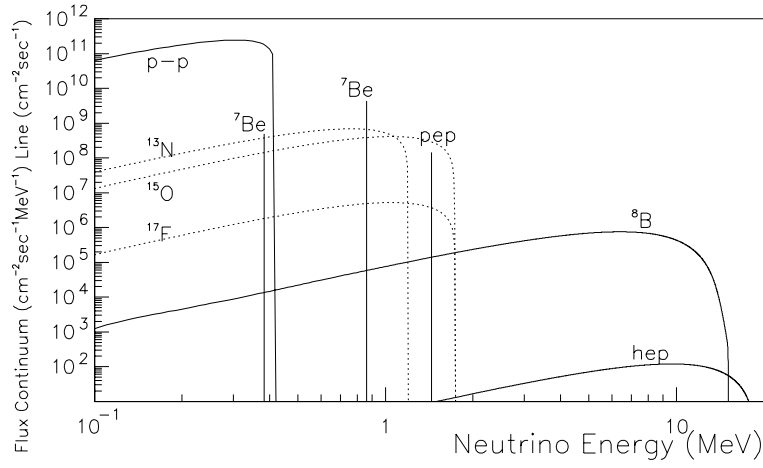


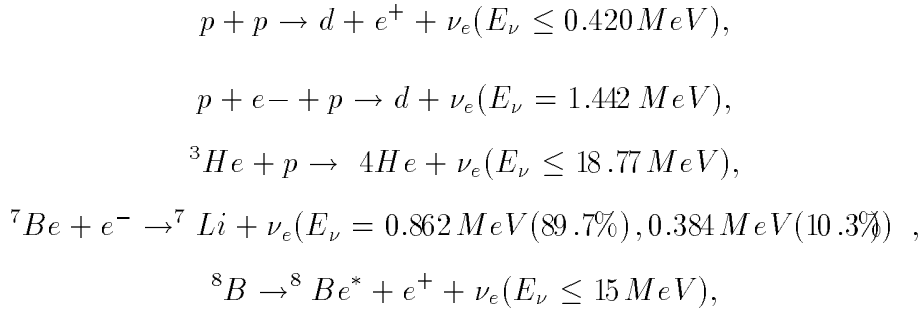
Figure 10: The solar neutrino spectra. KM and SK can only measure the ${}^8\text{B}$ -neutrinos and the Chlorine experiment can measure both the ${}^8\text{B}$ and ${}^7\text{Be}$ -neutrinos. The gallium experiments have lowest energy threshold and are able to observe neutrinos from the pp-fusion process which produces most of the solar neutrinos.

dotted lines which quite agree with the data.

It is interesting that a part of the allowed region can be accessible by planned long baseline neutrino oscillation experiments.

3.2 Solar Neutrinos

The solar neutrinos are produced in the central part of the sun through the various nuclear reactions [17]. The dominant processes producing neutrinos are those in the pp-chain:



The solar neutrino spectra predicted by a standard solar model is shown in figure 10.

The present energy threshold of SK is 6.5 MeV, and we therefore can only detect ${}^8\text{B}$ neutrinos, maximum energy of which is ~ 15 MeV.

The main interaction in this energy region is the neutrino electron elastic scattering, since the neutrino nucleus scattering is suppressed by the Pauli principle. The cross sections of the $\nu + e$ interactions are well calculated by the standard theory of the electro-weak interactions:

$$\frac{d\sigma}{dE_e} = \frac{2G_F^2 m_e}{\pi} \left[c_L^2 + c_R^2 \left(1 - \frac{E'_e}{E_\nu} \right)^2 + c_L c_R \frac{m_e}{E_\nu} \right],$$

where $c_L = 1/2 + \sin^2\theta_W$ and $c_R = \sin^2\theta_W$ for $\nu_e e$ scattering, and $c_L = -1/2 + \sin^2\theta_W$ and $c_R = \sin^2\theta_W$ for $\nu_\mu e$ scattering. The $\nu_e e$ interaction is mediated by both charged and neutral currents, and the $\nu_\mu e$ interaction is mediated only by the neutral current. With $\sin^2\theta_W = 0.225$, the total cross sections are

$$\sigma(\nu_e + e \rightarrow \nu_e + e) = 0.920 \times 10^{-43} (E_\nu/10 \text{ MeV}) \text{ cm}^2,$$

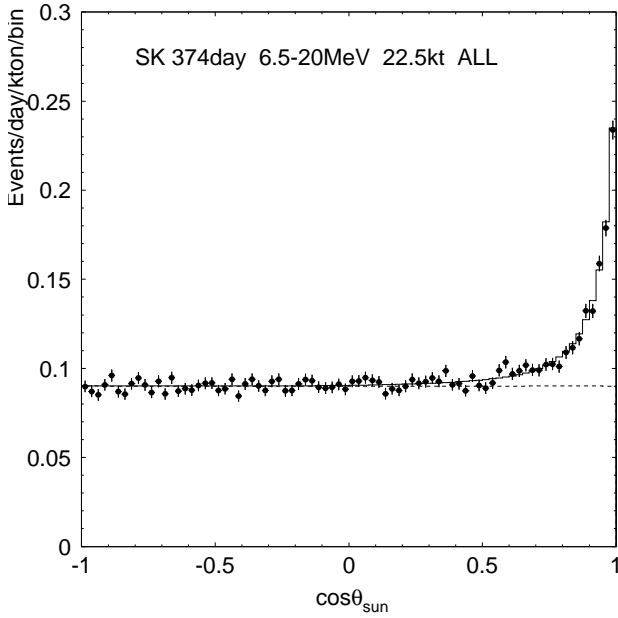


Figure 11: The $\cos\theta_{sun}$ distribution. The forward peak caused by the solar neutrino interaction is prominent.

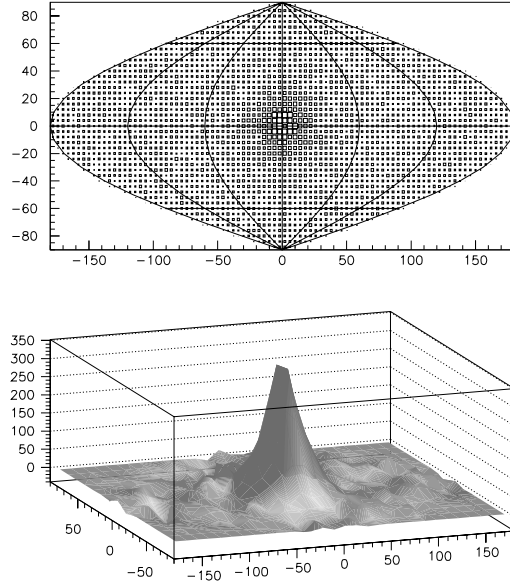


Figure 12: The image of the sun measured by the solar neutrino Neutrino Heliograph.

of reference[19] and for the likelihood calculation the data in the $\cos\theta_{sun}$ distribution are further divided into energy bins. The number of events thus obtained is 4,951.8 events in 374.2 days between 6.5 and 20 MeV in 22.5kt on fiducial volume.

The solar 8B neutrino flux is:

$$\phi_{sB} = 2.37^{+0.06}_{-0.05}(\text{stat.})^{+0.09}_{-0.07}(\text{sy st.}) \times 10^6 / \text{cm}^2 / \text{s},$$

Note that KM observed 597 events in 2079 days: the measured flux is $\phi_{sB} = 2.80 \pm 0.19(\text{stat.}) \pm 0.33(\text{sy st.}) \times 10^6 / \text{cm}^2 / \text{s}$. The result from SK agrees that from KM within experimental errors.

The ratio to the prediction of the standard solar model of BP95 is,

$$\frac{DATA}{SSM_{BP95}} = 0.358^{+0.009}_{-0.008}(\text{stat.})^{+0.014}_{-0.010}(\text{sy st.}).$$

The daytime and night-time flux difference has a solar model independent information on the large angle MSW solutions. The day and night flux ratio obtained by SK is,

$$\frac{(Day - Night)}{(Day + Night)} = -0.31 \pm 0.024(\text{stat.}) \pm 0.014(\text{sy st.}).$$

No significant overall flux difference is found. The effect of the regeneration through the earth depends upon the path length and the density profile of the earth where the solar neutrinos pass through. We therefore divided the night-data ($\cos\theta_z < 0.0$: the nadir is the z-coordinate) into five bins ($\Delta\cos\theta_z = 0.2$). We have shown in figure 13 the fluxes of daytime and night-time divided into 5 bins. The typical day/night fluxes expected from a large angle solution ($\Delta m^2 = 2.82 \times 10^{-5} eV^2$, $\sin^2 2\theta = 0.66$) and a small angle solution ($\Delta m^2 = 6.31 \times 10^{-6} eV^2$, $\sin^2 2\theta = 9.12 \times 10^{-3}$) of MSW effect are also plotted in figure 13.

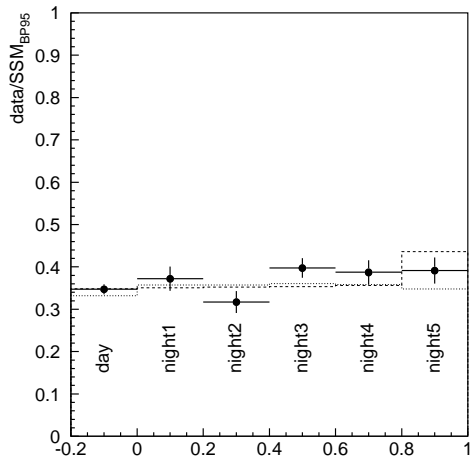


Figure 13: The day and night-time fluxes. The night data are divided into 5 bins with $\Delta\cos\theta = 0.2$. The expected day-night fluxes for $\Delta m^2 = 2.82 \times 10^{-5} eV^2$, $\sin^2 2\theta = 0.66$ (dashed line) and $\Delta m^2 = 6.31 \times 10^{-6} eV^2$, $\sin^2 2\theta = 9.12 \times 10^{-3}$ (dotted line) are shown.

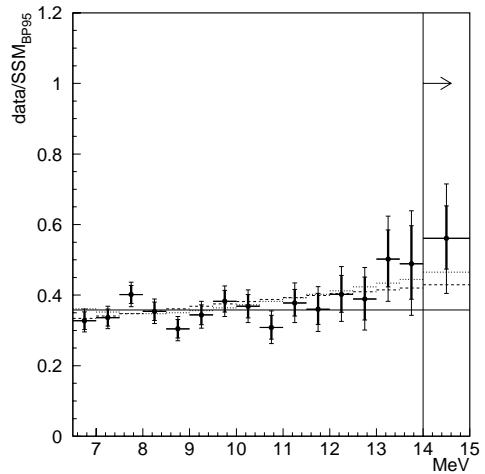


Figure 14: The spectrum of the recoil electrons. The thick parts show the statistical errors and the extensions with the thin bars show the combined error of statistical and systematic. Also shown are a typical small angle solution ($\Delta m^2 = 6.31 \times 10^{-6} eV^2$ and $\sin^2 2\theta = 9.12 \times 10^{-3}$ (dotted line)) and a typical just so solution ($\Delta m^2 = 7.08 \times 10^{-11} eV^2$ and $\sin^2 2\theta = 0.83$ (dashed line)).

By using the data we can study neutrino oscillation hypothesis. The confidence contour obtained is shown in figure 5 at 95% C.L. It is quite interesting to note that with this small data sample we can draw an excluded region for the half of the allowed region obtained by Hatada et al [20] are excluded.

The recoil electron energy spectrum is a key issue to understand the solution of the solar neutrino problem, since neutrino oscillation may have a strong energy dependence. It is especially to the so-called small angle solution and the just so vacuum oscillation. In figure 4, the spectrum of the recoil electrons is shown. The current data indicate that the distribution is consistent to be flat, but have better fit for a small angle or just so solution (namely non-flat distribution), although it is statistically significant. In figure 4, we also plot the expected energy distortion for a typical small angle ($\Delta m^2 = 6.31 \times 10^{-6} eV^2$ and $\sin^2 2\theta = 9.12 \times 10^{-3}$) and a just so solution ($\Delta m^2 = 7.08 \times 10^{-11} eV^2$ and $\sin^2 2\theta = 0.83$).

From the energy spectrum we can get the confidence contour for the neutrino oscillation parameter. For the MSW region we have obtained excluded region with 95% C.L. which is shown as a region surrounded by the solid curves in figure 5. For the just so region we have obtained excluded region at 99% confidence level but we get allowed region at 95% C.L. as shown in figure 6. However we should not take this seriously, this is not only because the statistics is not sufficient and the indication is very marginal but also because the SK experiment will soon increase the statistics rapidly in the next couple of years. We should wait a not very long time before the experiment can make a definite conclusion.

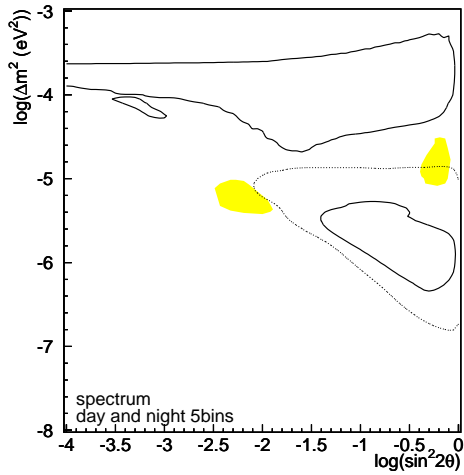


Figure 15: The confidence contour for the MSW effect by the SK data. The day/night flux difference and the electron energy distribution are used. No absolute flux information was used. The solid line shows the 95% excluded region by the energy spectrum and the dotted line shows the 95% excluded region by day/night data. Shaded regions are those obtained by Hata et al.

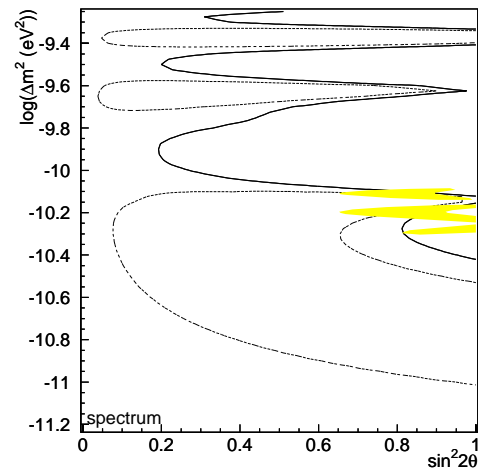


Figure 16: The confidence contour for the Just So oscillation obtained by the electron energy distribution. The solid line shows the region excluded by 99% C.L. and the dotted line shows the allowed region at 95% C.L.

References

- [1] The KM (II + II) collaboration consists of Uni v. of Tokyo, I CRR (Uni v of Tokyo), KEK, Tokai Uni v. Niiga Uni v. Gi f Uni v. To hoku Uni v. Ko be Uni v. Os aka Uni v. Tokyo Inst of Tech., I NS (Uni v of Tokyo), Mi ya gi Uni v of Educa ti on and Uni v of Pens y lva nia .
- [2] The Super -Ka mi o ka de col l ab at i on s i s t of I CRR (Uni v of Tokyo), KEK, To hoku Uni v., Tokai Uni v. Os aka Uni v. Ni i ga t Uni v. Tokyo Inst of Tech., Gi f Uni v. Mi ya gi Uni v of Educa ti o Ko be Uni v. Bos ton Uni v. Br o khaven Na ti on l ab or at or y Uni v of Cali for ni a (Ir vi ne) Cali for ni a Sta t Uni v. Geor ge Mas on Uni v. Uni v of Hawai i Los Al a mo Na ti on l ab. Louis i ana Sta t Uni v. s i t Uni v of Mary l and Sta t Uni v of New York (St y Br o k), Uni v of Wars w, and Uni v of Wash i ng ton.
- [3] K. Ari sa k et al . J. Phys . Soc . Jpn . 54, 3213 (1985) T. Kaji t æ et al . J. Phys . Soc . Jpn . 55, 711 (1986) K. S. Hi ra t æ et al . Phys . Let t B 220, 308 (1989) .
- [4] K. Hi ra t æ et al . Phys . Rev . Let t 58, 1490 (1987) .
- [5] K. S. Hi ra t æ et al . , Phys . Rev . Let t 65, 1297 (1990) K. S. Hi ra t æ et al . , Phys . Rev . D 44, 2241 (1991) ; D 45, 2170 E (1992) Hi ra t æ et al . Phys . Rev . Let t 66, 9 (1991) Y. Fukuda et al . , Phys . Rev . Let t 77, 1683 (1996) .
- [6] K. S. Hi ra t æ et al . Phys . Let t B 205, 416 (1988) ; S. Hi ra t æ et al . Phys . Let t B 208, 146 (1992) ; Y. Fukuda et al . , Phys . Let t B 335, 237 (1994) .

- [7] Physics and Astrophysics of Neutrinos., ed. by M.Fukugita and A Suzuki, p249, Springer-Verlag (1994).
- [8] Physics and Astrophysics of Neutrinos., ed. by MF ukugita and A Suzuki, p388, Springer-Verlag (1994).
- [9] These theses will be available in 6 months: Y. Koshio, Ph.D. thesis, University of Tokyo(1998); Y. Yaguchi, Ph.D thesis, Osaka University(1998); Okazawa, PhD thesis, Nigata University(1998); Kasuga, Ph.D thesis, University of Tokyo(1998); Hayato, Ph.D these, Tokyo Inst. of Technology .
- [10] Nakahata et al., to be published in Nucl. Instr. Methods.
- [11] L.Glashow et al., Phys. Lett. B190,199(1987).
- [12] H Albrecht et al., Phys. Lett. B202 (1988); H Albrecht et al., Phys. Lett. B292 (1992); D Baskulic et al., Phys. Lett. B359, 585 (1995).
- [13] K Asaragan et al., Phys. Rev. D3, 2065 (1996); K Asaragan et al., Phys. Lett. B35, 231 (1994).
- [14] Ch. Weinheimer et al., Phys. Lett. B300, 210 (1993); A I. Belev et al., Phys. Lett. B350, 263 (1995).
- [15] See for example, H V. Klapdor-Kingrothaus, in proceedings of the International Conference on Neutrino Physics and Astrophysics, Helsinki, 1996; Nucl. Physics. B(Proc. Suppl)48, 216 (1996).
- [16] S.Kasuga et al., Phys. Lett. B74, 238(1996).
- [17] see for example J.NBahcall and M.Hersonneault, Rev. Mod. Phys. 67,781(1995); S.Turck-Chièze and I.Lopes, Ap. J. 408,347(1993).
- [18] KInoue, in proceedings of TAUP97.
- [19] J.NBahcall et al., Phys. Rev. C54, 411 (1996).
- [20] NHita and P.Langacker, LASSNS-ASR 97/29, UPR751E, hep-ph/9705339, May (1997).